Design and fabrication of photonic crystal quantum cascade lasers for optofluidics

Marko Lončar, Benjamin G. Lee, Laurent Diehl, Mikhail Belkin, Federico Capasso

School of Engineering and Applied Sciences, Harvard University, 19 Oxford Street, Cambridge, MA 02138
loncar@deas.harvard.edu; capasso@deas.harvard.edu

Marcella Giovannini and Jérôme Faist

Institute of Physics, University of Neuchâtel, 1 Rue A.-L. Breguet, CH-2000, Neuchâtel, Switzerland

Emilio Gini

FIRST Center for Micro- and Nanoscience, Swiss Federal Institute of Technology, CH-8093, Zurich,, Switzerland

Abstract: We present novel designs and demonstrate a fabrication platform for electrically driven lasers based on high quality-factor photonic crystal cavities realized in mid-infrared quantum cascade laser material. The structures are based on deep-etched ridges with their sides perforated with photonic crystal lattice, using focused ion beam milling. In this way, a photonic gap is opened for the emitted TM polarized light. Detailed modeling and optimization of the optical properties of the lasers are presented, and their application in optofluidics is investigated. Porous photonic crystal quantum cascade lasers have potential for on-chip, intracavity chemical and biological sensing in fluids using mid infrared spectroscopy. These lasers can also be frequency tuned over a large spectral range by introducing transparent liquid in the photonic crystal holes.

OCIS codes: (140.5960) Semiconductor lasers; (140.4780) Optical resonators; (230.5750) Resonators; (140.3070) Infrared and far-infrared lasers; (140.3600) Lasers, tunable; (220.4000) Microstructure fabrication;

References and links,

1. F. Capasso, C. Gmachl, D. L. Sivco, and A. Y. Cho, "Quantum cascade lasers," Phys. Today **55**, 34 (2002)
2. C. Gmachl, F. Capasso, D. L. Sivco, and A. Y. Cho, "Recent progress in quantum cascade lasers and applications," Reports on Progress in Physics. **64**, 1533 (2001)
3. J. Faist, F. Capasso, C. Sirtori, D. L. Sivco, J. N. Baillargeon, A. L. Hutchinson, S. G. Chu, and A. Y. Cho, "High power mid-infrared (λ~5μm) quantum cascade lasers operating above room temperature," Appl. Phys. Lett. **68**, 3680 (1996).
4. S. Blaser, D. A. Yarekha, L. Hvozdara, Y. Bonetti, A. Muller, M. Giovannini and J. Faist, "Room-temperature, continuous-wave, single-mode quantum-cascade lasers at λ≈5.4μm," Appl. Phys. Lett. **86**, 041109 (2005).
5. L. Diehl, D. Bour, S. Corzine, J. Zhu, G. Höfler, M. Lončar, M. Troccoli and F. Capasso, "High-power quantum cascade lasers grown by low-pressure metal organic vapor-phase epitaxy operating in continuous wave above 400 K," Appl. Phys. Lett. **88**, 201115 (2006).
6. T. Yoshie, J. Vučković, A. Scherer, H. Chen, and D. Deppe, "High quality two-dimensional photonic crystal slab cavities," Appl. Phys. Lett. **79**, 4289-4291 (2001)
7. S. G. Johnson, S. Fan, A. Mekis and J. D. Joannopoulos, "Multipole-cancellation mechanism for high-Q cavities in the absence of a complete photonic band gap," Appl. Phys. Lett. **78**, 3388 (2001)
8. J. Vučković, M. Lončar, H. Mabuchi, and A. Scherer, "Design of photonic crystal microcavities for cavity QED," Phys. Rev. E **65**, 016608 (2002)
9. J. Vučković, M. Lončar, H. Mabuchi, and A. Scherer, "Optimization of the Q factor in photonic crystal microcavities," IEEE J. Quantum Electron. **38**, 850 (2002)
10. K. Srinivasan and O. Painter, "Momentum space design of high-Q photonic crystal optical cavities," Opt. Express **10**, 670 (2002)

#79184 - $15.00 USD Received 18 Jan 2007; revised 26 Mar 2007; accepted 27 Mar 2007; published 3 Apr 2007

11. K. Srinivasan, P. E. Barclay, O. Painter, J. X. Chen, A. Y. Cho and C. Gmachl, "Experimental demonstration of a high-quality factor photonic crystal microcavity," Appl. Phys. Lett. **83**, 1915 (2003)
12. Y. Akahane, T. Asano, B. S. Song and S. Noda, "High-Q photonic nanocavity in a two-dimensional photonic crystal," Nature **425**, 944 (2003)
13. D. Englund, I. Fushman and J. Vučković, "General recipe for designing photonic crystal cavities," Opt. Express **13**, 5961 (2005)
14. E. Kuramochi, M. Notomi, S. Mitsugi, A. Shinaya, T. Tanabe and T. Watanabe, "Ultrahigh-Q photonic crystal nanocavities realized by the local width modulation of a line defect," Appl. Phys. Lett. **88**, 041112 (2006)
15. T. Asano, B. S. Song and S. Noda, "Analysis of the experimental Q factors (similar to 1 million) of photonic crystal nanocavities," Opt. Express **14**, 1996 (2006)
16. O. Painter, R. K. Lee, A. Scherer, A. Yariv, J. D. O'Brien, P. D. Dapkus and I. Kim, "Two-dimensional photonic band-gap defect mode laser," Science **284**, 1819 (1999).
17. H. Y. Ryu, S. H. Kim, H. G. Park, J. K. Hwang, Y. H. Lee and J. S. Kim, "Square-lattice photonic band-gap single-cell laser operating in the lowest-order whispering gallery mode," Appl. Phys. Lett. **80**, 3883 (2002)
18. M. Lončar, T. Yoshie, A. Scherer, P. Gogna and Y. M. Qiu, "Low-threshold photonic crystal laser," Appl. Phys. Lett. **81**, 2680 (2002)
19. T. Yoshie, M. Lončar, A. Scherer and Y. Qiu, "High frequency oscillation in photonic crystal nanlasers," Appl. Phys. Lett. **84**, 3543 (2004).
20. H. Altug, D. Englund, and J. Vučković, "Ultrafast photonic crystal nanocavity laser," Nat. Phys. **2**, 484 (2006)
21. H. G. Park, S. H. Kim, S. H. Kwon, Y. G. Ju, J. K. Yang, J. H. Baek, S. B. Kim and Y. H. Lee, "Electrically driven single-cell photonic crystal laser," Science **305**, 1444 (2004)
22. A. Talneau, L. LeGratiet, J. L. Gentner, A. Berrier, M. Mulot, S. Anand, and S. Olivier, "High external efficiency in a monomode full-photonic-crystal laser under continuous wave electrical injection," Appl. Phys. Lett. **85**, 1913 (2004)
23. Demetri Psaltis, Stephen R. Quake, and Changhuei Yang, "Developing optofluidic technology through the fusion of microfluidics and optics," Nature **442**, 381 (2006)
24. L. Diehl, B. G. Lee, P. Behroozi, M. Lončar, M. A. Belkin, F. Capasso, T. Allen, D. Hofstetter, M. Beck and J. Faist, "Microfluidic tuning of distributed feedback quantum cascade lasers," Opt. Express **14**, 11660 (2006).
25. M. Lončar, A. Scherer and Y. Qiu, "Photonic crystal laser sources for chemical detection," Appl. Phys. Lett. **82**, 4648 (2003)
26. T. Yoshie, A. Scherer, J. Hendrickson, G. Khitrova, H. M. Gibbs, G. Rupper, C. Eli, O. B. Shchekin and D. G. Deppe, "Vacuum Rabi splitting with a single quantum dot in a photonic crystal nanocavity," Nature **432**, 200 (2004)
27. S. Strauf, K. Hennessy, M. T. Rakher, Y. S. Choi, A. Badolato, L. C. Andreani, E. L. Hu, P. M. Petroff and D. Bouwmeester, "Self-tuned quantum dot gain in photonic crystal lasers," Phys. Rev. Lett. **96**, 127404 (2006)
28. S. G. Johnson, S. H. Fan, P. R. Villeneuve, J. D. Joannopoulos, L. A. Kolodziejski, "Guided modes in photonic crystal slabs," Phys. Rev. B **60**, 5751 (1999).
29. R. Colombelli, K. Srinivasan, M. Troccoli, O. Painter, C. F. Gmachl, D. M. Tennant, A. M. Sergent, D. L. Sivco, A. Y. Cho and F. Capasso, "Quantum cascade surface-emitting photonic crystal laser," Science **302**, 1374 (2003).
30. K. Srinivasan, O. Painter, R. Colombelli, C. Gmachl, D. M. Tennant, A. M. Sergent, D. L. Sivco, A. Y. Cho, M. Troccoli and F. Capasso, "Lasing mode pattern of a quantum cascade photonic crystal surface-emitting microcavity laser," Appl. Phys. Lett. **84**, 4164 (2004).
31. C. L. Walker, C. D. Farmer, C. R. Stanley and C. N. Ironside, "Progress towards photonic crystal quantum cascade laser," IEE Proc. Optoelectronics **151**, 502 (204).
32. L. A. Dunbar, V. Moreau, R. Ferrini, R. Houdre, L. Sirigu, G. Scalari, M. Giovannini, N. Hoyler, and J. Faist, "Design, fabrication and optical characterization of quantum cascade lasers at terahertz frequencies using photonic crystal reflectors," Opt. Express **13**, 8960 (2005)
33. S. Hofling, J. Heinrich, H. Hofmann, M. Kamp, J. P. Reithmaier, A. Forchel and J. Seufert, "Photonic crystal quantum cascade lasers with improved threshold characteristics operating at room temperature,", Appl. Phys. Lett. **89**, 191113 (2006).
34. J. L. Jewell, J. P. Harbison, A. Scherer, Y. H. Lee and L. T. Florez, "Vertical-cavity surface-emitting lasers: design, growth, fabrication, characterization," IEEE J. Quantum Electtron. **27**, 1332 (1991).
35. Ph. Lalanne and J. P. Hugonin, "Bloch-wave engineering for high-Q small-V microcavities," IEEE J. Quantum Electron. **39**, 1430 (2003)
36. J. Melngailis, "Focused ion-beam technology and applications," J. Vac. Sci. Tech. B **5**, 469 (1987).
37. M. J. Cryan, M. Hill, D. Cortaberria Sanz,, P. S. Ivanov, P. J. Heard, L. Tian, S. Yu and J. M. Rorison, "Focused ion beam-based fabrication of nanostructured photonic devices," IEEE, J. Sel. Top. Quantum Electron. **11**, 1266 (2005).
38. A. Chelnokov, K. Wang, S. Rowson, P. Garoche, J. M. Lourtioz, "Near-infrared Yablonovite-like photonic crystals by focused-ion-beam etching of macroporous silicon," Appl. Phys. Lett. **77**, 2943 (2000).
39. J. Schilling, J. White, A. Scherer, G. Stupian, R. Hillebrand, U. Gosele, "Three-dimensional macroporous silicon photonic crystal with large photonic bandgap," Appl. Phys. Lett. **86**, 011101 (2005).
40. M. Lončar, B. G. Lee, M. Troccoli, L. Diehl, F. Capasso, M. Giovannini, J. Faist, "Novel photonic crystal quantum cascade laser platform," CLEO 2006.
41. L. Hvozdara, A. Lugstein, N. Finger, S. Gianordoli, W. Schrenk, K. Unterrainer, E. Bertagnolli, G. Strasser, and E. Gornig, "Quantum cascade lasers with monolithic air-semiconductor Bragg reflectors," Appl. Phys. Lett. **77**, 1241 (2000).

#79184 - $15.00 USD Received 18 Jan 2007; revised 26 Mar 2007; accepted 27 Mar 2007; published 3 Apr 2007

42. K. E. Zinoviev, C. Dominguez, A. Vila, "Diffraction grating couplers milled in Si_3N_4 rib waveguides with a focused ion beam," Opt. Express **13**, 8618 (2005).
43. Y. Fu and N. K. A. Bryan, "Investigation of physical properties of quartz after focused ion beam bombardment," Appl. Phys. B **80**, 581 (2005).
44. M. L. Adams, M. Lončar, A. Scherer and Y. M. Qiu, "Microfluidic integration of porous photonic crystal nanolasers for chemical sensing," IEEE J. Sel. Areas Commun. **23**, 1348 (2005).
45. E. Chow, A. Grot, L. W. Mirkarimi, M. Sigalas and G. Girolami, "Ultracompact biochemical sensor built with two-dimensional photonic crystal microcavity," Opt. Lett. **29**, 1093 (2004)
46. J. Topolancik, P. Bhattacharya, J. Sabarinathan and P. C. Yu, "Fluid detection with photonic crystal-based multichannel waveguides," Appl. Phys. Lett. **82**, 1143 (2003).
47. H. Kurt and D. S. Citrin, "Photonic crystals for biochemical sensing in the terahertz region," Appl. Phys. Lett. **87**, 041108 (2005).
48. D. Erickson, T. Rockwood, T. Emery, A. Scherer and D. Psaltis, "Nanofluidic tuning of photonic crystal circuits," Opt. Lett. **31**, 59 (2006)
49. C. Sirtori, F. Capasso, J. Faist, A. L. Hutchinson, D. L. Sivco, A. Y. Cho, "Resonant tunneling in quantum cascade lasers," IEEE J. Quantum Electron. **34**, 9 (1998).
50. J. Z. Chen, Z. Liu, Y. S. Rumala, D. L. Sivco and C. F. Gmachl, „Direct liquid cooling of room-temperature operated quantum cascade lasers," Electron. Lett. **42**, 534 (2006).
51. J. E. Bertie and K. H. Michaelian, "Comparison of infrared and Raman wave numbers of neat molecular liquids: which is the correct infrared wave number to use?," J. Chem. Phys. **109**, 6764 (1998)

1. Introduction

Recent progress in semiconductor crystal growth techniques has enabled the realization of materials with engineered electronic and optical properties. This is the most notable in the case of quantum cascade lasers (QCLs) where controlled growth of semiconductor layers with nanometer-scale thickness enables lasing action in mid- and far-infrared wavelength range [1-5]. Mid-infrared (MIR) QCls operating in the 5 to 10 μm range have achieved room temperature operation with high output powers and single mode capabilities that have made them the source of choice for chemical and biological sensing applications. At the same time, nanofabrication techniques have evolved to a precision that allows realization of optical resonators capable of storing photons in ultra-small volumes for long periods of time. Recent advances in the design and fabrication of photonic crystal (PhC) cavities have resulted in tremendous improvement of the quality factor (Q) available in these optical resonators [6-15]. PhCs cavities with $Q\sim10^6$ and mode volumes on the order of a cubic wavelength of light [$V_{mode}\sim(\lambda/n)^3$] offer great promise for the realization of low-threshold, high-speed, single-mode lasers [16-20]. In order for these nanolasers to find application it is important to achieve room-temperature operation using electrical injection [21, 22]. One of many applications of PhC nanolasers is optofluidics, an emerging technology that combines photonics with microfluidics for increased functionality [23]. In one scheme the analyte, with characteristic MIR absorption, dissolved in a transparent carrier fluid would be microfluidically delivered into the laser cavity to perform on-chip spectroscopy. In another scheme, transparent fluids with controlled refractive indices would be introduced in the cavity in order to realize tunable lasers with large tuning range. Recently, using this approach, our groups have demonstrated microfluidic tuning of a distributed feedback (DFB) QCL [24].

In this work, we present the results of numerical simulation and the fabrication of novel MIR PhC QCLs designed for efficient current injection. Our structures take advantage of both electric bandgap engineering (quantum cascade structure) and photonic bandgap engineering (photonic bandgap structure) to enable realization of compact, highly-integrated MIR laser sources that can be used as sensors in an intra-cavity [25] configuration for lab-on-a-chip platform. However, our approach is general and can be used to realize efficient current injection in PhC diode lasers emitting, for example, at telecom wavelengths.

#79184 - $15.00 USD Received 18 Jan 2007; revised 26 Mar 2007; accepted 27 Mar 2007; published 3 Apr 2007

2. Design of High-Q Photonic Crystal Cavities for Quantum Cascade Lasers

One of the most promising applications of planar PhCs is the realization of optical cavities with high Q and small V_{mode}. In comparison to other types of optical cavities, PhC cavities can achieve both of these requirements simultaneously, which makes them interesting candidates for low-threshold lasers. Quality factors as high as $Q\sim10^6$ [15] have been recently demonstrated in planar PhC nanocavities defined in passive material (e.g. silicon) with no gain and no significant material losses. The Q in this case is limited by out-of plane scattering losses. When the cavity is defined in active materials, Q decreases due to re-absorption of light in the sections of PhC that are not pumped. The highest Q reported in active materials is ~20,000 [26, 27]. The free-carrier absorption, due to large doping levels in PhC cavities that are designed for electrical injection, can further decrease the maximum available Q.

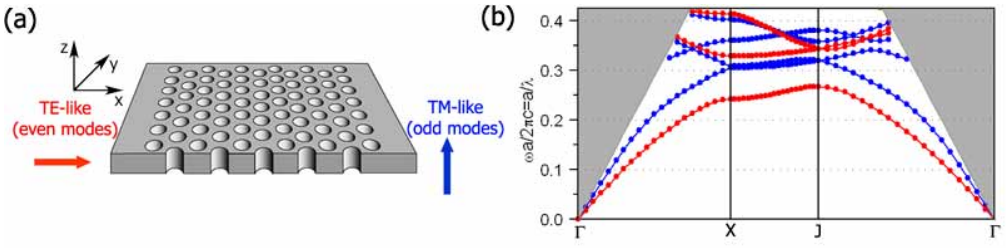

Fig. 1. (a) Schematic of a thin-slab PhC structure. Guided modes of the structure can be even (TE-like) or odd (TM-like) with respect to the symmetry plane in the middle of the slab (z=0). Even modes have E-field perpendicular to the holes at z=0 and odd modes have E-field parallel to the holes at z=0. (b) Band diagram for guided modes of InP slab (n_{InP}=3.09 @ λ=5.8μm) perforated with holes of radius *r=0.28a*. Slab thickness is *t=0.75a*, *a* is periodicity of the lattice. Bandgap is open for even modes (red), and it is closed for odd modes (blue).

In this work we consider a thin-slab PhC platform (Fig. 1). Such a structure supports a photonic bandgap for modes with even symmetry with respect to the plane in the middle of the slab [28]. In the middle of the slab these modes have E-field polarized perpendicular to the plane of the holes (TE-like polarization).

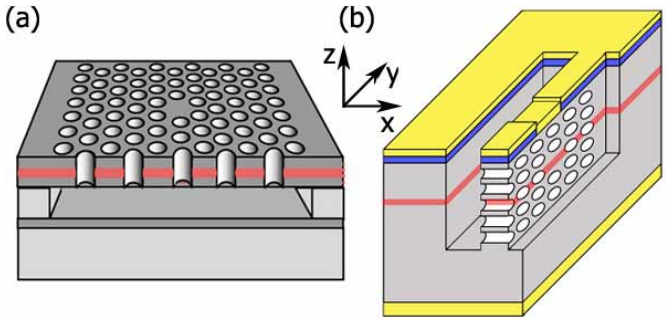

Fig. 2. (a) Schematic of conventional planar PhC laser, with holes etched perpendicular to the top surface. (b) Novel design, based on a thin vertical slab perforated with holes parallel to the top surface. The active region is shown in red, metal contacts in yellow, and the insulating silicon nitride in blue.

The light generated in QCLs is TM-polarized, with the E-field polarized along the z-axis (i.e. along the direction of crystal growth). Therefore, the structure with holes etched into the top surface of the sample, as it is typically done [Fig. 2(a)], does not support a photonic bandgap for TM-polarized light emitted from the QCLs. Laser action in such a structure is still possible due to the distributed feedback provided by the photonic crystal lattice that plays a role of a two-dimensional grating and was recently reported [29, 30]. However, in order to take full advantage of PhC cavities (i.e. high Q, small V_{mode}, large spontaneous emission

#79184 - $15.00 USD Received 18 Jan 2007; revised 26 Mar 2007; accepted 27 Mar 2007; published 3 Apr 2007

factor) it is necessary to open a photonic bandgap. One way to achieve that is to use the lattice of rods in air [31-33] since such a structure supports a photonic bangap for TM polarized light [28]. However, such a system could suffer from the lack of vertical confinement of light and limited Q factors.

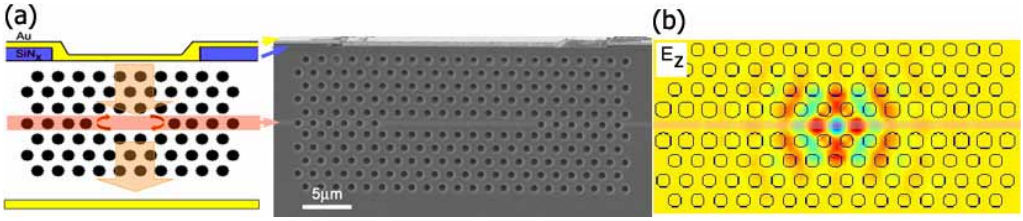

Fig. 3. (a) Schematic of the proposed laser design and scanning electron microscopy (SEM) micrograph of the fabricated structure. All electrons that are injected in the structure travel through the active region and participate in light generation. Quantum wells can be seen as a light gray stripe in the SEM image. (b) Simulation result of the high-Q "heterostructure" cavity. Active region is not perforated with PhC lattice, resulting in reduced surface recombination.

In order to open a photonic bandgap for TM polarized light in thin-slab PhCs, holes need to be etched along the x-axis, perpendicular to the growth direction and parallel to the surface of the sample. The schematic of the structure that we propose is shown in Fig. 2(b). In this structure TM-polarized light has the E-field perpendicular to the plane of the holes and a photonic bandgap is open. It is interesting to compare our structure to vertical cavity surface emitting lasers (VCSEL) [34] that incorporate epitaxially grown distributed Bragg mirrors below and above quantum wells to achieve light confinement. Similarly to VCSELs and in contrast to conventional PhC lasers, our design enables efficient current injection and eliminates re-absorption of the emitted light in the mirrors since the active region extends in the cavity only (Fig. 3). To summarize, advantages of the proposed design are:

1. **Efficient current injection.**
   Metal contacts are positioned exactly above the cavity, and all injected electrons participate in the light generation, thus reducing the leakage and threshold currents.
2. **Reduced optical losses (re-absorption of light) in PhC mirror**
   The active region (gain) exists only in the region with missing holes (i. e. cavity), and re-absorption in the mirror section is eliminated. In contrast, in conventional PhC lasers active region extends throughout the photonic crystal mirror [Fig. 2(a)].
3. **Reduced surface-recombination**
   Using the "heterostructure" cavity design [Fig. 3(b)] [15], it is possible to realize high-Q cavities without perforating the quantum wells. This can reduce non-radiative surface recombination that can be a significant problem in PhC lasers due to the large surface to volume ratio. Surface recombination, however, is not an issue for QCLs due to their unipolar nature.

The material that we used in this work is designed to operate at λ=5.8μm. It is based on the structure reported by Faist et al. [3, 4] with the following modifications: (i) the active region consists of only 10 stages instead of 30 stages, (ii) the inner InGaAs waveguide cladding layer, typically used to improve the mode confinement factor (Γ), is not grown. Both modifications result in the reduced Γ in our structure. This was done intentionally in order to simplify the material growth considering that Γ will be improved using PhC mirrors above and below the active region. Table 1 summarizes the QCL structure used in our experiments. The active region was grown using molecular beam epitaxy (MBE) using InAlAs/InGaAs material system latticed matched to InP substrate. The thick InP cladding on top of the active region was grown using metal-organic chemical vapor deposition (MOCVD). This thick cladding (7μm instead of typical 1-3μm) is needed to accommodate the PhC mirror.

#79184 - $15.00 USD Received 18 Jan 2007; revised 26 Mar 2007; accepted 27 Mar 2007; published 3 Apr 2007

Table 1. The structure of the QCL material. The active region consists of 10 stages. One stage consists of the following InGaAs/InAlAs layer sequence: 2.7/ **2.2**/ 2.5/ **2.0**/ 2.2/ **2.0**/ 2.1/ **2.3**/ 2.2/ **2.7**/ 2.1/ **3.0**/ 2.0/ **4.3**/ 1.3/ **1.9**/ 5.2/ **1.8**/ 4.5/ **2.8**/ 2.8/ **2.1.** The layer thicknesses are given in nanometers. InAlAs barriers are shown in bold. The underlined numbers correspond to the doped layers with doping level $4\cdot10^{17}$cm^{-3} resulting in the averaged doping of the active of 10^{17}cm^{-3}. *n* is the real and *k* is the imaginary part of the refractive index.

#	Material	Thickness [nm]	Description	Doping [cm^{-3}]	*n*	*k*
6	InGaAs	50	Contact	10^{19}	2.22	$4.9\cdot10^{-2}$
5	InGaAs	500	Contact	$7\cdot10^{18}$	2.87	$2.9\cdot10^{-2}$
4	InP	7000	Cladding	10^{17}	3.09	$9.4\cdot10^{-5}$
3	InAlAs/InGaAs	15	Graded Interface	$3\cdot10^{17}$	3.30	$3.8\cdot10^{-4}$
2	Active (10 stages)	567	Active	10^{17}	3.32	$1.2\cdot10^{-4}$
1	InAlAs/InGaAs	29.7	Graded Interface	$3\cdot10^{17}$	3.32	$4.0\cdot10^{-4}$
	InP (substrate)		Cladding	10^{17}	3.09	$9.4\cdot10^{-5}$

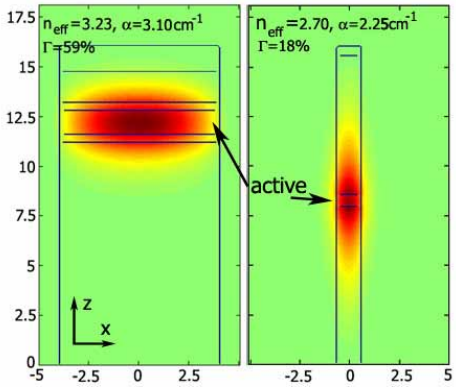

Fig. 4. E_z component of the fundamental mode of a (a) 8μm wide ridge made in a conventional QCL material [25], and (b) 1.2μm wide waveguide made in modified QCL material. Two layers above and below active region in (a) are the inner cladding InGaAs layers used to improve Γ. The axes are labeled in μm.

In Fig. 4 we show the distribution of E_z component of the fundamental mode in the ridge waveguides made in conventional (ridge width is 8μm) and modified (ridge width is 1.2μm) QCL materials. We chose to work with narrow ridge in the case of the modified QCL structure, which supports only one transverse-mode. This is done in order to open a photonic bandgap, as it is known that higher order transverse-modes can close the photonic bandgap [28]. The confinement factor, calculated using Equation 1, is Γ=59% in the conventional design and Γ=18% in the modified one. The effective mode index and propagation loss (material absorption) of the modified QCL waveguide are n_{eff}=2.7 and $\alpha_{waveguide}$=2.25cm^{-1}, respectively. Here we used a more general definition of Γ than the one commonly used in semiconductor lasers, namely:

$$\Gamma = \int_{active} W_z\,dxdz \Big/ \int_{total} W_{tot}\,dxdz,\quad W_z = \varepsilon E_z^2,\quad W_{tot} = \varepsilon(E_x^2 + E_y^2 + E_z^2) \tag{1}$$

Equation 2 shows the dependence of the laser threshold current density (J_{th}) on total losses of the laser (both material and mirror losses, $\alpha = \alpha_{waveguide} + \alpha_{mirror}$) and gain (g) of the material.

$$J_{th} = \frac{\alpha}{g\Gamma} \tag{2}$$

In order to reduce the threshold current of the laser (Equation 2) it is important to maximize Γ. In the case of conventional photonic crystal *diode* lasers, that emit TE-like

#79184 - $15.00 USD Received 18 Jan 2007; revised 26 Mar 2007; accepted 27 Mar 2007; published 3 Apr 2007

polarized light (i.e. E-field has only E_x and E_y components), we are often not concerned with the structure optimization that maximizes Γ. This is due to the fact that both E_x and E_y can couple to the dipole in order to enable stimulated emission. In the case of QCLs however, the emitted radiation originates from intersubband transitions and as such is z-polarized (TM polarization). Therefore we are interested in PhC structures that preserve the polarization of the emitted light. In Fig. 5 we show two possible implementations of the PhC structure above and below the active region (boundaries indicated by two black lines). We use a three-dimensional finite difference time domain (3D FDTD) code with cubic grid to study these structures. In Fig. 5(a) the active region extends in the ΓJ direction of PhC, while in Fig. 5(b) it extends in the ΓX direction. The parameters of both structures are: r/a=0.28, t/a=0.52, n_{active}=3.33, n_{InP}=3.09, where a=1.75μm is the periodicity of the lattice, r is the radius of holes and t is the width of the slab. In both cases the quantum well region thickness is t_{QW}=0.7μm. It can be seen that the structure shown in Fig. 5(a) couples the E_z component strongly to the E_y component thus reducing Γ (=13%). On the other hand, the ΓX waveguide shown in Fig. 5(b) does not couple strongly E_z to E_y, resulting in a larger overlap factor (Γ=42%). It is interesting to note that the structure based on ΓJ waveguides has a smaller confinement factor than the as-grown structure (Γ=18%). Clearly, care needs to be taken when designing QCL PhC cavities in order to maximize Γ. Note that the confinement factor can be further improved by incorporating more quantum wells and increasing the width of the slab and the thickness of active region. For example, a conventional QCL structure with ~1.5μm thick active region could have near unity confinement factor in the ΓX configuration. In the rest of this section we will consider thicker structures that have t/a=0.75

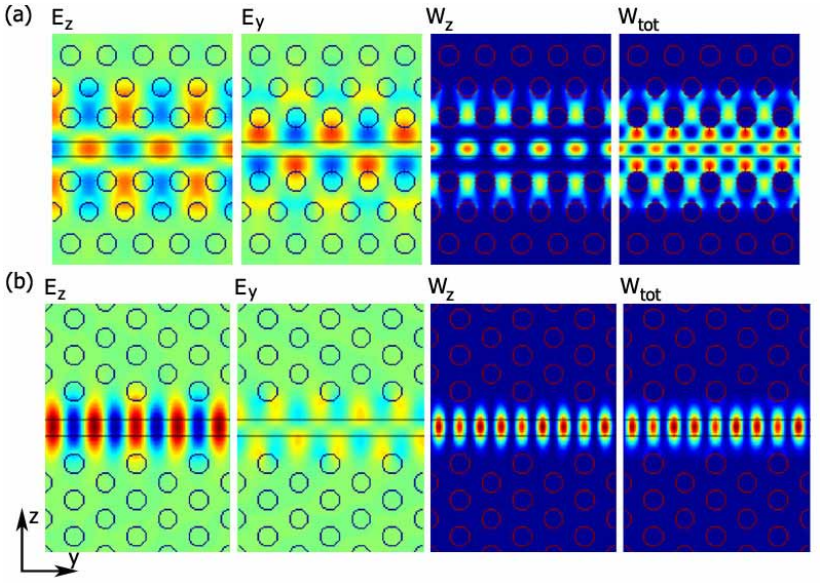

Fig. 5. Two possible implementations of PhC structure below and above active region. (a) ΓJ and (b) ΓX waveguides. (a) ΓJ waveguide couples strongly E_z and E_y components of the field, thus reducing confinement factor. (b) ΓX waveguide preserves the polarization of the E_z field emitted by QCL structure. Modes are shown for k vector at the edge of Brillouin zone: (a) a/λ=0.289 (b), a/λ=0.34 (λ is wavelength in air).

Next, we investigate cavities based on ΓJ and ΓX waveguide designs discussed above. The Q of PhC cavity can be broken down into partial quality factors that describe different energy loss mechanisms:

#79184 - $15.00 USD Received 18 Jan 2007; revised 26 Mar 2007; accepted 27 Mar 2007; published 3 Apr 2007

$$\frac{1}{Q}=\frac{1}{Q_{scattering}}+\frac{1}{Q_{material}}\quad=\frac{1}{Q_x}+\frac{1}{Q_y}+\frac{1}{Q_z}+\frac{1}{Q_{material}} \tag{3}$$

Radiation loss in the z direction (Q_z) can further be separated into the radiation losses towards the top contact ($Q_{contact}$) and radiation losses towards the substrate ($Q_{substrate}$): $1/Q_z=1/Q_{contact}+1/Q_{substrate}$. Also, we distinguish between radiation in the positive (y+) and negative (y-) direction of y-axis ($1/Q_y=1/Q_{y+}+1/Q_{y-}$). In a conventional PhC cavity one is concerned only with the losses due to out of plane scattering (Q_x in our case), since in plane losses can be significantly reduced by incorporating large number of PhC layers (Q_z, $Q_y \rightarrow \infty$). However, this cannot be done in our system in which the number of PhC layers that can be accommodated between the top metal contact and the active region is limited to 4 or 5 due to the finite thickness of the top InP cladding. This puts an upper limit on the total quality factor that can be achieved in our system. It should be mentioned that $Q_{substrate}$ can be made higher than $Q_{contact}$ since the bottom cladding is formed by the InP substrate and can be thick. Material absorption is another limiting factor for the total Q of the PhC cavity. $Q_{material}$ in a conventional, ridge-waveguide QCL can be written as

$$Q_{material}=\frac{2\pi n_{eff}}{\lambda\alpha_{waveguide}}=\frac{n_{eff}}{2k_{eff}}, \tag{4}$$

where n_{eff} and k_{eff} are the real and imaginary part of the effective mode index, respectively, andand $\alpha_{waveguide}$ is the absorption loss in the waveguide in units of cm^{-1}. Using the parameters calculated for the narrow ridge-waveguide shown in Fig. 4 (n_{eff}=2.7, α=2.25cm^{-1}) we obtain $Q_{material}$~13,000.

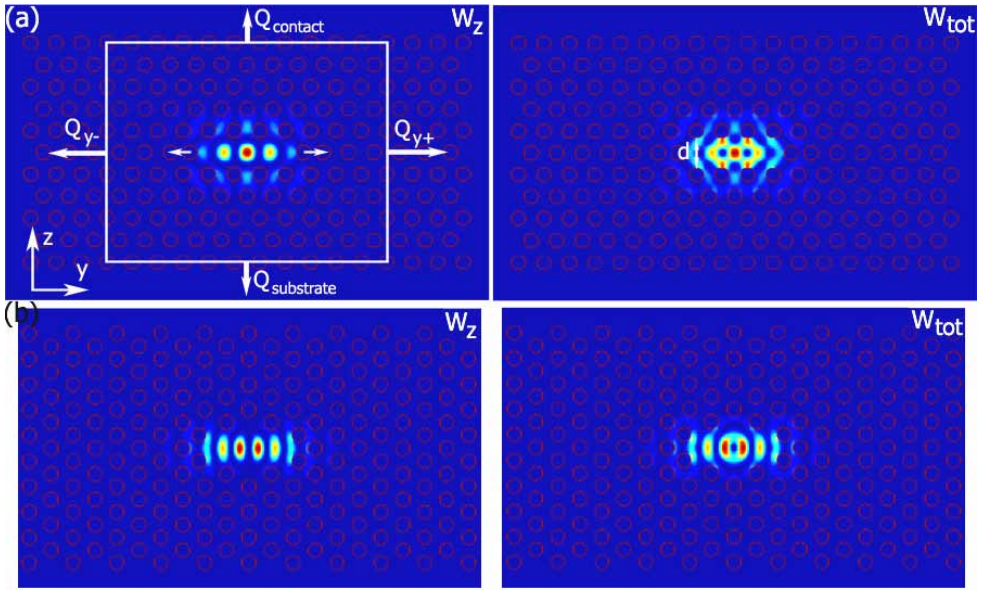

Fig. 6. (a) Resonant mode in the cavity based on the design in Reference 12. The cavity resonance and Q are tuned by shifting holes, as indicated by arrows, and by controlling the width of the cavity, d, by moving the photonic crystal mirrors above and below the cavity towards the center of the cavity. A white box outlines the region used to calculate the partial Qs. (b) Cavity based on ΓX waveguide. The same mechanism as in (a) is used to tune the cavity Q and the resonant frequency.

In addition to achieving large Q and large Γ, the laser cavity should be designed to have large extraction efficiency. Assuming the emission in the x-direction, this means that Q_x should be smaller than both Q_y and Q_z in order to extract the most of the light generated in the

#79184 - $15.00 USD Received 18 Jan 2007; revised 26 Mar 2007; accepted 27 Mar 2007; published 3 Apr 2007

laser. Otherwise, significant amount of light will be emitted towards the contact and substrate and will be lost. The extraction efficiency of the PhC cavity can be estimated from

$$\eta_i = \frac{1/Q_i}{1/Q} \tag{5}$$

where $i=x$, y or z, depending on the direction of the light extraction.

In Fig. 6(a) we show a cavity based on the design first proposed by Noda's group [12]. The parameters of the structure are: t=1.4μm, a=1.65μm, r/a=0.28, grid=60nm. By shifting the two holes on y-axis (small white arrows) away from the center of the cavity, it is possible to control the Q_x of the cavity. In order to push the mode deeper in the photonic bandgap, and thus increase Q_z and Q_y, the width of the cavity (d) is controlled by moving top and bottom PhC mirrors towards the center of the cavity. Using these two tuning parameters we were able to achieve Q_x in the range of 5,000 to 180,000 and $Q_{contact}$ in the range of 20,000 to 90,000. For example, cavity with a shift of 360nm and the mirrors moved by 240nm has Q_z≈41,000, Q_y≈57,000, Q_x≈52,000 resulting in total Q≈16,000 (material losses are neglected) and the extraction efficiency of η_x=30.8%. The extraction efficiency can be further improved by extracting the light in other directions. For example, it is possible to reduce the number of PhC layers left of the cavity and therefore reduce Q_{y-} to <10,000 while maintaining high Q_{y+}. For example, Q_{y-} of 5,000 and Q_z=41,000, Q_{y+}=114,000 and Q_x=52,000 result in total Q~4,000 and η_{y-}=79%. In all cases, the confinement factor is around Γ≈20%.

Next, we explore the influence of the material loss on the cavity Q. First, we increased the number of PhC mirrors in the z-direction to 8 layers, and in y-direction to 9 layers, in order to increase the total cavity Q. In this case we used r/a=0.3. The cavity with the hole shift of 360nm and the mirrors moved by 60nm was studied. Without the material absorption, the total Q was ~57,000. When the material absorption was included (per Table 1), the total Q dropped to ~13,000. Therefore, we estimate $Q_{material}$ to be around $Q_{material}$≈17,000. The 30% increase in $Q_{material}$ from the one predicted using Equation 4 (narrow ridge without holes) can be attributed to reduced overlap between light and lossy semiconductor due to the presence of the holes.

In Fig. 6(b) we show an alternative cavity design, based on ΓX waveguide. The best Q that we were able to achieve in this structure, using tuning mechanism similar to the one described in the previous case, was Q_x~5,000 while maintaining Q_y=111,000 and Q_z=18,000. This results in Q_{total}=3,800 and η_x=76%. As expected, this cavity also has larger confinement factor of Γ=32%. Q_z in this structure can be improved using slightly larger holes (e.g. r/a=0.3 instead of r/a=0.28).

For comparison, we also calculate Q in conventional Fabry-Perot type QCL that is 1mm long and has one facet coated with gold (reflectivity R_{back}=100%) and the other facet is cleaved (R_{front}=30%). Neglecting the material losses we find Q=6,000 using following expression:

$$Q = \frac{2\pi n_{eff}}{\lambda \alpha_{mirror}} = 2\pi n_{eff} \frac{L}{-\lambda \ln\left(\sqrt{R_{front} R_{back}}\right)} \tag{6}$$

where α_{mirror} are mirror losses of the cavity. The total Q, including material absorption losses for the conventional QCL ($Q_{material}$~11,300) is Q_{total}~4,000. As it can be seen, PhC cavities can be designed to have Q comparable to or higher than those found in conventional ridge-waveguide QCLs. However, PhC QCLs are much more compact and are two orders of magnitude smaller than traditional QCLs. Therefore, we expect the threshold current to be significantly reduced in PhC QCLs. Moreover, due to the large spontaneous emission factor (β factor) that is typical in PhC cavities (e.g. see Reference 27), threshold current will be further reduced.

Next, we consider a different type of PhC cavity that is based on a 4μm wide ridge made in a conventional QCL material. The structure, shown in Fig. 7(a), is a Fabry-Perot cavity with PhC mirrors instead of cleaved facets. In this case, the confinement of light in z-direction is achieved by the refractive index contrast between active region and InP cladding. The

#79184 - $15.00 USD Received 18 Jan 2007; revised 26 Mar 2007; accepted 27 Mar 2007; published 3 Apr 2007

reflectivity of cleaved semiconductor facet is on the order of 30% and therefore mirror losses of a Fabry-Perot cavity are large unless the cavity is long (Equation 6). We propose to use PhC mirrors instead of cleaved facet in order to reduce mirror losses. In Fig. 7(b) we show the reflection and transmission of light through photonic crystal mirror consisting of 8 layers of photonic crystal fabricated in a t=4μm wide ridge (a=1.3μm, r/a=0.3). Since such a ridge waveguide is multimode, higher order transverse modes could in principle close the bandgap and reduce the reflectivity. However, Fig. 7b shows that this is not the case, and more than 95% of light in the fundamental mode, incident on the PhC mirror is reflected back into the fundamental mode. This is due to the fact that a perfect PhC mirror (holes with vertical sidewalls) cannot couple the fundamental mode to higher order transverse modes. In Fig. 7(c) we show the reflectivity assuming slanted sidewalls (i.e. conical holes) with angle 4° off the normal (typical for focused ion beam milling). It can be seen that reflectivity drops to ~90%. We attribute this to the coupling of the fundamental mode into the higher order transverse modes due to the reduced symmetry of the structure due to tapered holes. Indeed, when the ridge width is reduced to t=2μm the reflectivity approaches 100% even for tapered holes.

An increase of the mirror reflectivity from 30% to 95% means that cavity length can be reduced ~25 times, maintaining the same quality factor of the laser cavity. The ultimate goal of this approach is the realization of very short FP cavities ($L \sim \lambda/n_{eff}$) with low mirror losses and high Q. This can be achieved using tapered mirror designs proposed by Lalanne et al [35].

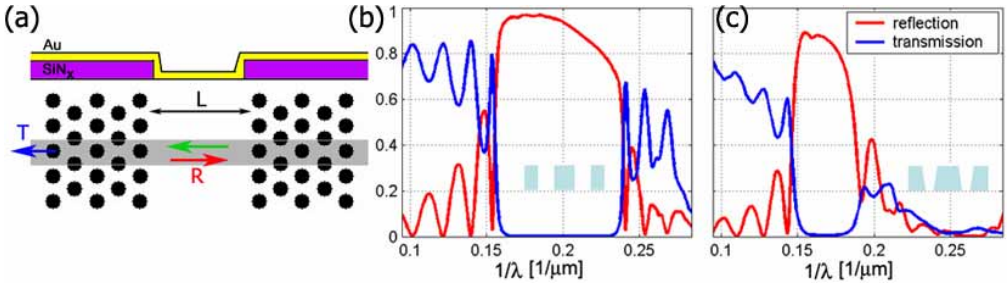

Fig. 7. (a) Fabry-Perot cavity with photonic crystal mirrors. (b) and (c) The reflectivity and transmission of a photonic crystal mirror consisting of 8 layers of holes made in a 4μm -thick slab. Holes are assumed to have have (b) vertical side walls or (c) slanted side walls (4°).

3. Fabrication of photonic crystal quantum cascade lasers

Our PhC QCLs are made using a combination of conventional dry-etching techniques and a focused ion beam (FIB) milling [36]. This allows us to achieve the three-dimensional sculpting needed to realize our lasers with PhC fabricated on the sides of the vertical semiconductor slabs (waveguide ridges). The fabrication procedure (Fig. 8) starts with the growth of semiconductor material described in Table 1. Then, a 300nm thick silicon nitride insulating layer is deposited using Electron-Cyclotron Resonance (ECR) plasma-enhanced chemical-vapor deposition (PECVD). Photolithography, followed by wet chemical etching (buffered hydrofluoric acid), is used to define openings in the silicon nitride that serve as metal contacts on top of the cavity. Next, metal layers for the top contact are evaporated (20nm Ti/ 600nm Au) and the sample is spin-coated with a thin sacrificial Omnicoat layer (Microchem) followed by 5μm thick SU-8 2005 photoresist (Microchem). Omnicoat is used to enable SU-8 removal after the fabrication is completed, since SU-8 cannot be easily dissolved. Next, SU-8 is patterned using a contact photolithography, and t=1.4μm wide ridges as well as bonding pads are defined. Argon ion milling is then used to transfer the mask from SU-8 into the metal. Then, ECR reactive ion etching (RIE) in CF_4 chemistry is used to transfer the mask into the silicon nitride layer and is followed by ECR RIE etching to transfer the mask into the semiconductor. The final semiconductor etch is done using hydrogen-chlorine chemistry. The conditions that we used are: hydrogen flow of 9sccm, chlorine flow

#79184 - $15.00 USD Received 18 Jan 2007; revised 26 Mar 2007; accepted 27 Mar 2007; published 3 Apr 2007

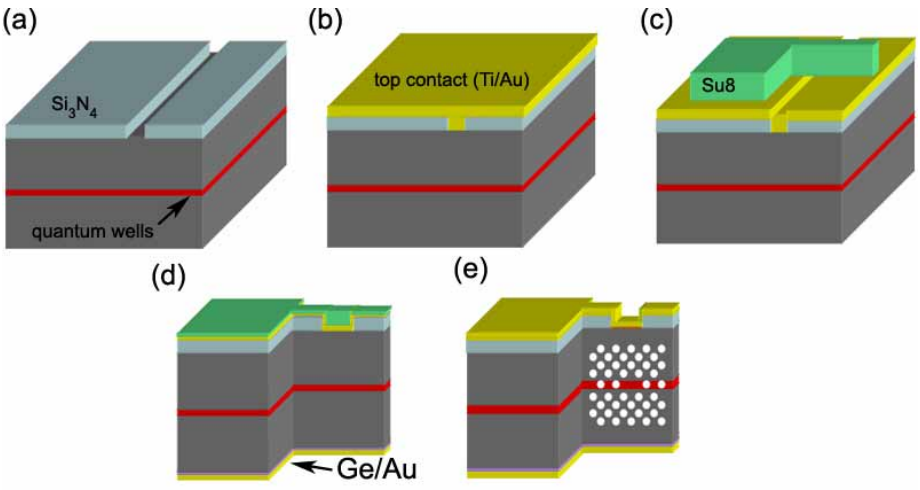

Fig. 8. Fabrication sequence. See text for detailed description.

of 11sccm, ECR power of 800W, RF powerof 250W and DC bias of -220V. The etch rates that we obtain in our system are ~1μm/min, with selectivity InP:Su8 = 5:1. We found that SU-8 resist is a very good etch mask for H/Cl chemistry. As seen in Fig. 9, we are able to etch 20μm tall semiconductor slabs, with vertical and optically smooth side walls using our recipe. Once the dry etching is done, SU-8 photoresist is removed from the sample by removal of the sacrificial Omnicoat layer. The sample substrate is then polished down to ~200 μm thickness and the bottom metal contact (10nm of Ge/ 200nm of Au) is deposited.

Next, the PhC cavity is defined on the side of the vertical slab using FIB. FIB milling is a mask-less dry-etching technique originally developed for repair of photolithography masks as well as for preparation of samples for transmission electron microscopy. Recently, it has been successfully used to realize photonic devices in InGaAsP materials [37]. The most exciting feature of FIB milling is its ability to achieve three-dimensional sculpting since it allows fabrication on structures at any angle with respect to the surface of the sample, in contrast to conventional planar fabrication technology. This has been successfully utilized in the realization of 3D PhC [38, 39] as well as QCLs [40, 41]. In addition, FIB milling allows rapid prototyping of photonic devices.

Our FIB system (FEI DB235 FIB/SEM dual beam system) uses Ga^+ ions to perform milling. Ion beam can also be used to image the structure and locate quantum wells prior to milling. This allows us to position the PhC cavity precisely around the active region and achieve good overlap between the cavity mode and the gain material (Figs. 3 and 9). Due to the physical nature of the milling process, photonic crystal holes fabricated with FIB in the bulk semiconductor material have slanted walls with sidewall angle ~4° (conical, v-shape profile). This is due to the re-deposition of the milled (excavated) material on the sidewalls. As seen in the previous section, conical holes can reduce the reflectivity of the PhC and significantly decrease the Q of the cavities. However, in the case of PhC fabricated in the narrow-ridge, the sidewall angle is significantly reduced since the sputtered material can be removed forward once the ridge is completely perforated. In addition, FIB can also be used to mill multiple structures that are lined up in a row [Fig. 9(c)]. The sidewall angle can be further reduced, if necessary, by depositing a hard-mask made of silicon nitride on the side of the slab. This silicon nitride layer (~100nm thick) also plays a positive role in reducing the material damage from the exposure to the ion beam during the imaging with ions. Without it, Ga^+ gets implanted into the material [42, 43] during the imaging process required to align the photonic crystal cavity to the quantum wells. This thin sheet of implanted Ga forms a conductive layer that can shunt the QCL. We monitored, in-situ, the resistance of our lasers during ion imaging and noticed the reduction in the ohmic resistance as the structure gets

#79184 - $15.00 USD Received 18 Jan 2007; revised 26 Mar 2007; accepted 27 Mar 2007; published 3 Apr 2007

exposed to the ion beam. The silicon nitride layer can be removed at the end using wet etching.

Ga^+ ions with energy of 30kV and te beam current of 300pA were used to mill the PhC structure. The time needed to mill one hole in a 1.4μm wide ridge is ~3sec, and the whole PhC cavity can be fabricated in about 10min. Milling time increases for the wider ridges. In Fig. 9(a) we show one structure with four different PhC cavities fabricated in the same ridge. In this case, all structures are connected to the same bonding pad (in parallel). Using FIB, it is

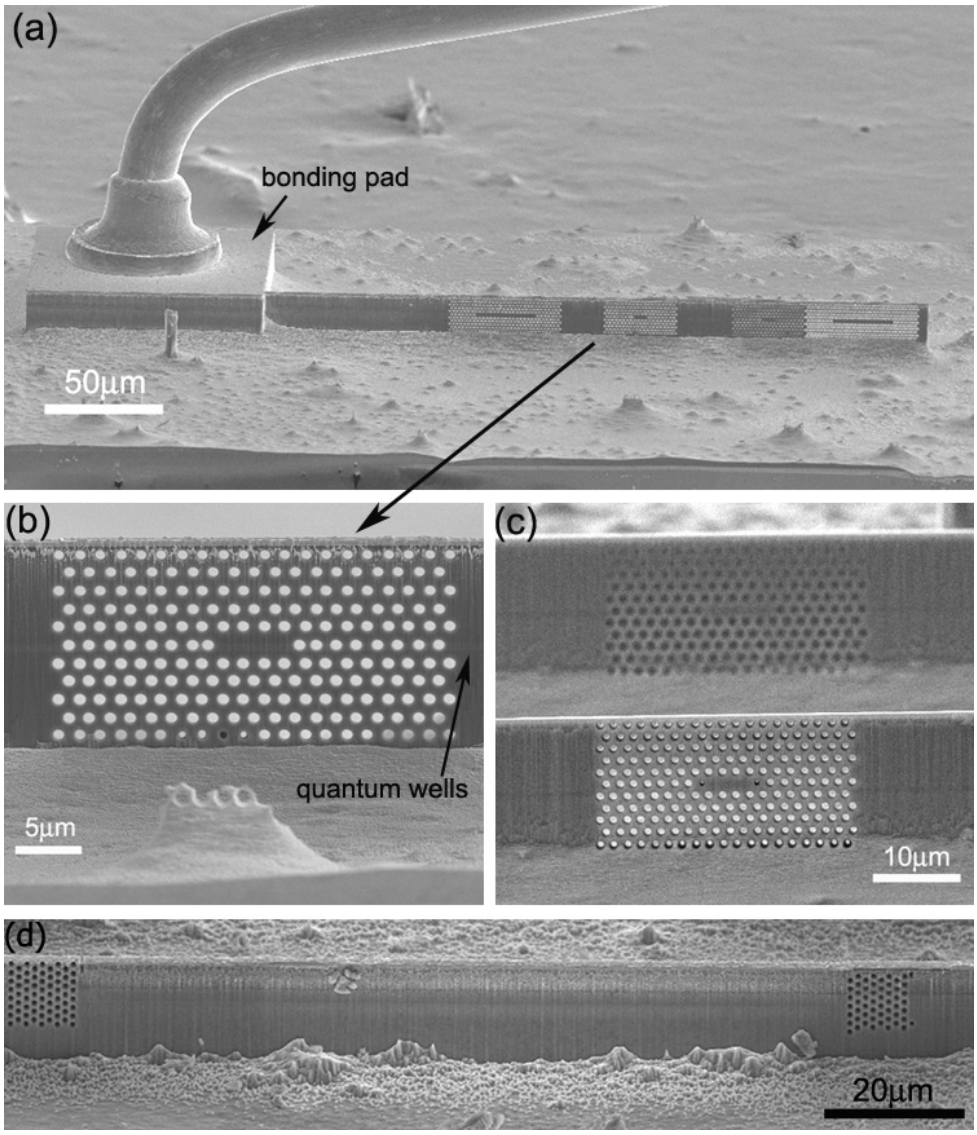

Fig. 9. Fabricated PhC cavities. (a) The structure consisting of a bonding pad and a thin ridge with four different cavities. (b) Blow-up of a ΓJ cavity. The quantum well active region can be seen as a light-gray stripe, indicated by an arrow. (c) SEM image of another structure. (d) Fabry-Perot cavity formed between the two photonic crystal mirrors.

possible to subsequently disconnect the cavities one by one if needed. In Fig. 9(b) we show a blow-up of one of the cavities. The cavity is the same as the one that we modeled using 3D FDTD [Fig. 6(b)]. It can be seen that photonic crystal cavity is very well aligned to the active region seen as a light gray stripe in the center. In Fig. 9(c) we show another fabricated

#79184 - $15.00 USD Received 18 Jan 2007; revised 26 Mar 2007; accepted 27 Mar 2007; published 3 Apr 2007

structure. Here we fabricated two narrow ridges 250μm apart. First, the ridge in front is milled using FIB. Once the Ga^+ beam completely perforates the front ridge, it travels through the holes and continues milling the second ridge (seen in the background). It can be seen that the cavity in the second ridge is also very well aligned to the active region, even though the two ridges are 250μm apart. This demonstrates that the ion beam is parallel to the surface of the sample and that the depth of focus of the ion beam is sufficiently large so that multiple PhC cavities (one behind another) can be fabricated in parallel.

Another interesting application of FIB is "trimming" of fabricated structures. For example, after the initial testing, a fabricated structure can be further modified in order to, for example, tune the emission wavelength of the laser (e.g. enlarge some holes). It is also possible to define cavities that are emitting in the y direction instead of the x direction, as discussed above, simply by milling away several layers of the photonic crystal mirror.

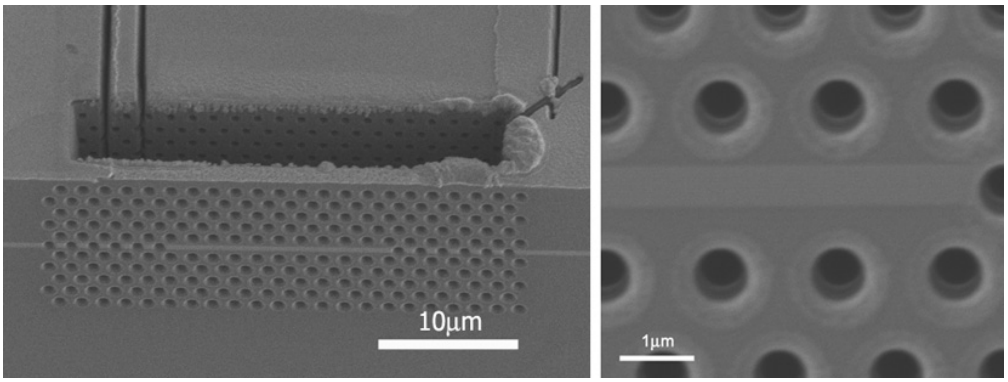

Fig. 10. Photonic crystal cavity fabricated using FIB only (no dry etching).

FIB can also be used to fabricate the complete PhC QCL, without the need of dry etching. Even though this procedure is somewhat time consuming it is interesting for rapid testing of different PhC designs. The sample is first cleaved and then a deep trench is milled next to the cleaved facet using FIB (Fig. 10). In this case, one side of the vertical slab is defined by cleaving and is atomically flat, and the other side is defined by FIB milling. This procedure is similar to the procedure of making TEM samples using FIB. Finally, the PhC cavity is defined on the edge of the sample, precisely around quantum wells (Fig. 10).

The fabricated structures were tested using electrical injection. Lasing action was observed in Fabry-Perot cavities [Fig. 9(d)] at low temperatures and under pulsed injection. Due to poor power efficiency of QCLs (presently of the order of 4% at room temperature) most of the injected power is converted into heat that needs to be dissipated over t=1.4μm wide ridge. This poor heat dissipation leads to an increase in the threshold current and forces the laser to be operated in pulsed mode with low duty cycle.

To this date we have not observed lasing action from compact photonic crystal cavities [Fig. 9(b) and (c)]. We believe that this is due to the mismatch between gain spectrum of QCL material and resonance of fabricated PhC cavities, that can be attributed to the precision with which we can control the size (r) and the periodicity (a) of holes in PhC lattice. This is related to the resolution of our FIB that uses 12-bit digital to analog converter (total 4096 pixels in y and z direction) to register position and size of the holes.

4. Applications of Photonic Crystal Quantum Cascade Lasers to Optofluidics

Due to their porous nature, PhCs are very interesting for sensing applications in the intra-cavity configuration [25, 44-48]. It has already been demonstrated that cavity resonance and Q depend strongly on the refractive index of the environment, that is on the refractive index of the fluid into which the laser is immersed [25]. By integrating lasers within microfluidic channels [5, 25, 44] it is possible to realize widely tunable lasers in which the emission

#79184 - $15.00 USD Received 18 Jan 2007; revised 26 Mar 2007; accepted 27 Mar 2007; published 3 Apr 2007

wavelength is controlled by the refractive index of the surrounding fluid. Recently, we have demonstrated this approach on conventional distributed feedback QCLs [5] and obtained tunability of $\Delta\lambda/\Delta n_{fluid}$=10nm/REU (refractive index unit). Here we show that the tuning range can be significantly larger in the case of optofluidic PhC QCLs.

In Fig. 11(a) we show a schematic of the proposed optofluidic system that can achieve multiple functions: (i) a tunable laser with large tuning range, (ii) a sensor for absorption spectroscopy and (iii) a system for cooling PhC lasers [49]. The PhC QCL, based on the design shown in Fig. 6(a), is embedded in a microfluidic channel, made of PDMS, using techniques that were developed earlier [5, 44]. By introducing non-absorbing fluids with refractive index in the range $n_{fluid} \in (1.3, 1.7)$ into the microfluidic channel, the emission wavelength of the laser can be tuned from λ=5.85μm to λ =6.11μm. That is, the tunability of PhC QCL is $\Delta\lambda/\Delta n_{fluid}$=650nm/REU [Fig. 11(b)]. This wide tuning range comes at the expense of increased threshold current due to the reduced Q of the cavity: Q drops from about Q≈5,000 (n_{fluid}=1.3) to Q≈500 (n_{fluid}=1.7). The reduction is due to increase of out-of-ridge light leakage due to the reduced index contrast between the ridge material and the surrounding fluid.

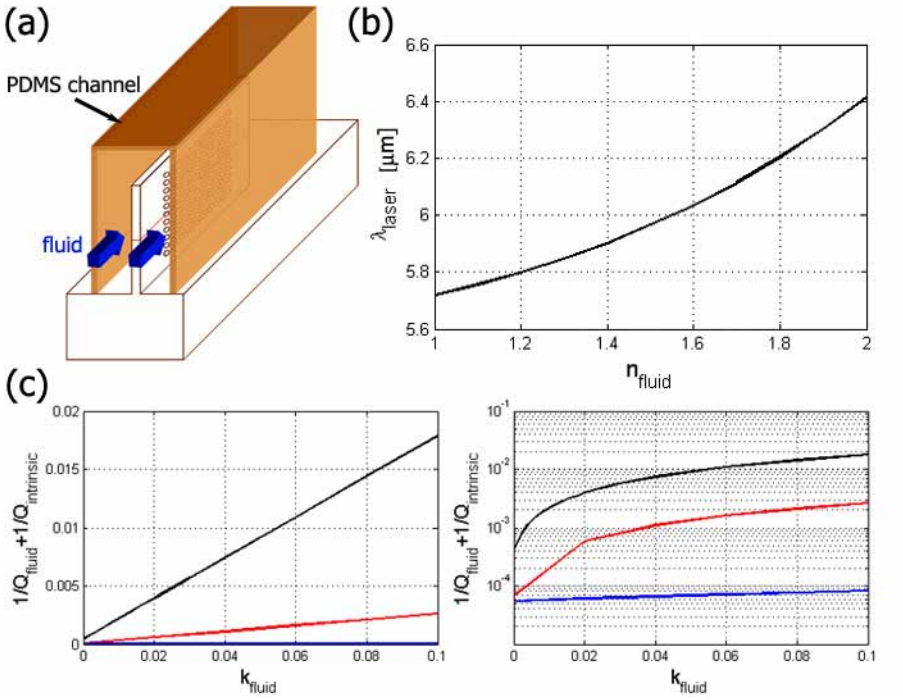

Fig. 11. (a) Schematic of PhC QCL integrated with microfluidic channel. (b) Emission wavelength of the laser vs. refractive index of the fluid surrounding the laser. (c) $1/Q=1/Q_{intrinsic}+1/Q_{fluid}$ of laser immersed in fluid as a function of imaginary part of the refractive index of the fluid. Black line – PhC QCL, red line 1.4μm wide conventional QCL, and blue line 8μm wide conventional QCL. Both linear and semi-log scales are shown.

Perhaps, the most interesting application of PhC QCL is in chemical/biological sensing using infrared absorption spectroscopy. It is known that many molecules of interest have signature absorption at MIR wavelengths. Due to the compact nature of the proposed PhC QCLs it is possible to integrate a number of lasers on the same chip. These lasers can have predetermined emission wavelength tuned to specific absorption lines of the molecules of interest. The analyte, which is either an absorbing fluid or a solution of absorbing molecules in a non-absorbing carrier fluid, can be delivered *in situ* into the laser cavity. The presence of

#79184 - $15.00 USD Received 18 Jan 2007; revised 26 Mar 2007; accepted 27 Mar 2007; published 3 Apr 2007

absorbing analyte increases the laser threshold, due to increased absorption losses, and reduces the laser output power. This mechanism enables the realization of compact sensors based on PhC QCLs capable of detecting small volumes of analytes. In Fig. 11(c) we show the dependence of inverse of the total Q ($1/Q=1/Q_{fluid}+1/Q_{intrinsic}$) on the imaginary part of the refractive index of the analyte for three different lasers: (i) PhC QCL with ridge width t=1.4 μm, (ii) narrow-ridge traditional QCL with ridge width t=1.4μm, and (iii) wide-ridge traditional QCL with ridge width t=8μm. 1/Q for conventional QCLs is calculated using Equation 4, and does not include the mirror losses. 1/Q in the case of PhC QCL includes material losses and all scattering losses. In all cases we assume that non-absorbing fluid with $n_{fluid}=1.4$ is used as a carrier to bring small amounts of absorbing analyte into the laser cavity. Therefore, the imaginary part of the refractive index (k) of the solution depends on the concentration of the analyte. It can be seen that PhC QCL is the most sensitive to the changes in absorption of the analyte. The dependence of total 1/Q on k is linear and can be written as

$$\frac{1}{Q}(k)=\frac{1}{Q_{\text{int}rinsic}}+\frac{1}{Q_{fluid}}=\frac{1}{Q_{\text{int}rinsic}}+k\cdot S \qquad (7)$$

where S is the slope of the curve. We find that $S_{PhC}=0.1734$, $S_{narrow}=0.0255$, $S_{wide}=2.7\text{x}10^{-4}$. From equations 2, 4 and 6 we see that laser threshold current density is proportional to inverse quality factor $J_{th}\sim 1/Q$. We can therefore write $J_{th}(k)/J_{th}(0)=1+\delta k$, where $\delta=S\cdot Q_{intrinsic}$. We find $\delta_{PhC}=416$, $\delta_{narrow}=38$ and $\delta_{wide}=0.5$ Therefore, by measuring precisely the threshold current of the laser it is possible to determine k and therefore the amount of analyte in the carrier fluid. Note that the threshold current can be determined without an additional optical detector, simply by monitoring the position of the characteristic kink observed in the differential resistance of QCL at threshold [50].

Next, we estimate the reduction in the output power of the laser when immersed in a small amount of absorbing analyte dissolved in the carrier fluid. For example, this method could be used for detection of acetone in a carrier fluid. Acetone has an absorption peak at λ=5.83μm (C=O stretch) with absorption coefficient $\alpha_{acetone}=9{,}000\ \text{cm}^{-1}$ [51], resulting in $k_{acetone}=0.43$. Assuming a 0.05% acetone solution in a transparent fluid (resulting in $k=2\text{x}10^{-4}$) we find that the PhC QCL will experience 8% increase in the threshold current, compared to the threshold current in carrier fluid only (no acetone). The 8% increase in the threshold current can produce a major change on the emitted optical power, particularly if the laser is operated close to threshold. Then, even a small amount of absorbing analyte can completely shut-off the laser. For example, let us assume that the laser is operated at constant current $I=1.1\text{x}I_{th}(k=0)$, and that the output power is $P_{out}(k=0)$. Assuming that the slope-efficiencies with and without analyte are the same, we find that 8% increase in the threshold current results in the 5-fold reduction in the output power $P_{out}(k)=0.2*P_{out}(k=0)$. (Note: slope efficiency will experience an 8% decrease due to increased total losses). Significantly larger sensitivity is expected if the laser is operated below-threshold, in the exponential region of the P_{out}-I curve.

5. Conclusions

We have designed and demonstrated a novel "holey" semiconductor laser platform based on electrically driven photonic crystal quantum cascade lasers with efficient current injection. Our approach takes advantage of electronic bandgap and photonic bandgap engineering to realize novel, compact, mid-infrared laser sources. We have demonstrated that a combination of photonic crystal lasers and microfluidic delivery system can result in compact widely tunable mid-infrared lasers that are suitable for chemical and biological sensing based on mid-infrared spectroscopy. Our optofluidic platform could also function as an ultracompact detectorless lab-on-chip in which the analyte detection is achieved by monitoring the changes in the laser threshold current.

#79184 - $15.00 USD Received 18 Jan 2007; revised 26 Mar 2007; accepted 27 Mar 2007; published 3 Apr 2007

Acknowledgments

The Harvard University group acknowledges financial support from DARPA Optofluidic Center under grant number HR0011-04-1-0032. Fabrication has been carried out in Center for Nanoscale Systems (CNS) at Harvard University. We would like to acknowledge help from Mariano Troccoli, Sindy Tang, Warren Moberlychan, Richard Schalek, and John Tsakirgis.

#79184 - $15.00 USD Received 18 Jan 2007; revised 26 Mar 2007; accepted 27 Mar 2007; published 3 Apr 2007